Second International Symposium on Marine Propulsors
smp'11, Hamburg, Germany, June 2011

# Application of Vortex Confinement Method in Combination with Two-Way Euler-Lagrangian Coupling Approach for the Prediction of Cavitating Propeller Tip Vortex Flows

**Thomas Hachmann[1], Moustafa Abdel-Maksoud[2], Dieter Hänel[3], Udo Lantermann[4]**

[1]OBERMEYER Planen + Beraten GmbH, Munich, Germany
[2]Institute for Fluid Dynamics and Ship Theory (FDS), Hamburg University of Technology (TUHH), Hamburg, Germany
[3]Institute of Combustion and Gas Dynamics, University of Duisburg-Essen, Duisburg, Germany
[4]Institute of Ship Technology, Ocean Engineering and Transport Systems, University of Duisburg-Essen, Duisburg, Germany

## ABSTRACT

The present work deals with investigations of numerical aspects in vortex dominated flows.

Computations of realistic technical configurations require efficient methods and a high-grid resolution, which is not sufficient in most cases to capture important details of the flow. Insufficient resolution increases the numerical dissipation of vortices generated at the tip region of lifting surfaces. One possible solution to reduce the unphysical decay of the strength of the vortices (despite moderate solution) is the application of vorticity confinement methods (Steinhoff 1994).

The aim of this work is to restrict the artificial manipulation of the flow field to only special areas of interest. The vorticity confinement formulation is therefore coupled to vortex detection methods in order to restrict the influence only to dominating vortices. Two methods for vortex line detection based on a predictor corrector scheme are used (Banks 1995). The predictor step is in both cases dependent on the vorticity. The corrector step is once based on the pressure magnitude and/or the vorticity magnitude and once based on the velocity field. The result in both cases is a characteristic representing of the core of the vortex.

A two-way Euler-Lagrangian concept is applied to study the cavitation behavior of tip vortices of propellers. This concept is based on the definition of volume fractions, derived from the bubble distribution inside and around a computational cell. The applied two-way coupling allows the consideration of the movement and dynamics of single vapor bubbles. The applicability of developed methods is demonstrated for one propeller geometry.

### Keywords

Vorticity confinement, vortex flow, propeller, vortex detection, cavitation

## 1 INTRODUCTION

Investigations of vortex dominated flows are of interest in many scientific and technical problems. In the attempt to achieve comparable results to measured values, especially in a cavitating flow, the computation effort for vortex dominated flows is still very high. Numerical techniques to reduce vortex dissipation in non-highly resolved meshes have been performed and showed good results for different vortex dominated flows.

Aim of the present paper is the development of a vorticity confinement method in combination with a vortex detection algorithm to restrict the artificial manipulation of the flow field to only areas of interest. The manipulated flow field is additionally coupled to a two-way Euler-Lagrange based cavitation model.

## 2 VORTICITY CONFINEMENT IN COMBINATION WITH VORTEX DETECTION

### 2.1 Vorticity Confinement

The basic idea of vorticity confinement methods is to add anti-diffusive terms to the momentum equations of the fluid. The momentum equation is:

$$\frac{\partial v}{\partial t} + (v \cdot \nabla)v = \frac{1}{\rho}\nabla p + \mu \nabla^2 v - \varepsilon s \qquad (1)$$

with the confinement term $s$ and a control parameter $\varepsilon$. The confinement term consists of a vector $\hat{n}$ pointing to the center of the vortex and a scalar, which is dependant on the vorticity or alternatively on the helicity.

This formulation is presented for many test cases in the literature. The vorticity and the helicity-based formulation lead to problems in flows where the boundary layer is modeled. The vorticity in the boundary layer is often higher than the vorticity in regions where vorticity confinement is requested. This leads to numerical problems in the solution. The calculation gets instable before differences can be seen in regions where vorticity confinement is requested.

A formulation by Robinson et al (Robinson 2004) is used in this paper. Robinson's idea was to split the source term $s$ in a part giving the direction of the anti-dissipative source and a part giving the strength of the anti-dissipative source:

$$s = \rho|\omega|\left[\frac{\nabla|\omega|}{|\nabla|\omega||} \times \frac{\omega}{|\omega|}\right] \quad (2)$$

The part giving the direction of the source can be found in the square brackets.

### 2.2 Vortex detection

The vortex confinement formulation by Robinson et al (Robinson 2004) affects the whole computational region. This leads to instabilities in regions where no additional source term is required and, accordingly, not requested. Therefore, the VC formulation is coupled with a vortex detection method to reduce and specify the affected area in more detail.

The predictor-corrector-technique by Banks & Singer (Banks 1995) is used to identify the vortex core by discrete points. The vortex detection scheme is based on two steps:

1. Seed point determination
2. Vortex tracing

The seed point detection takes place in the area downstream of the propeller where strong vortices are expected. A plane is spanned in this area defined by the main flow direction as normal vector and the expected core radius as edge length. This is done interactively. The plane is afterwards partitioned in a Cartesian grid and scanned for the minimum pressure and maximum vorticity to define the seed point. For practical reasons it is not advised to place the plane in areas where the vortex comes into existence, but rather, in areas downstream where the vortex is already fully developed and isolated.

The tracing of the vortex center is again based on two steps. A predictor step followed by a corrector step. The corrector step is similar to an Euler-integration in vorticity direction.

The vortex core is located in a region along the vorticity vector. Figure 1 shows the schematic sequence of the predictor step.

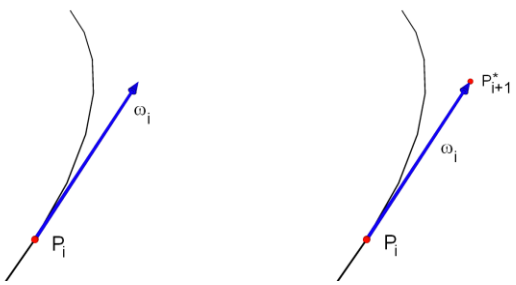


**Figure 1: Predictor step**

Point $P$ is the starting point with the corresponding vorticity vector $\omega_i$. Point $P^*_{i+1}$ shows the predicted point after the integration. A correction of this point is necessary as this is only a rough estimation and does not represent the vortex core. The integration in vorticity direction is limited by the local cell size to reduce errors by large integration steps.

The following corrector step corrects the coordinates of Point $P^*_{i+1}$ based on a minimum pressure formulation. A plane is spanned through Point $P^*_{i+1}$ with the local vorticity vector $\omega^*_{i+1}$ as normal vector. The location of the pressure minimum in this plane represents the corrected coordinates of point $P_{i+1}$.The sequence of the corrector scheme can be seen in Figure 2.

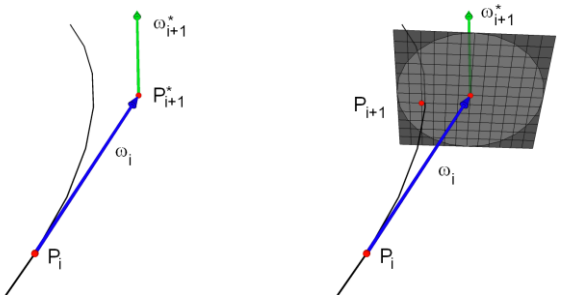


**Figure 2: Corrector step**

Point $P^*_{i+1}$ represents the predicted point with its corresponding vorticity $\omega^*_{i+1}$. Point $P_{i+1}$ represents the corrected point. The analysis plane is reduced by the local vortex core radius to reduce the computational effort. Interpolations for the corrector step take only place in the circular region of the analysis plane.

Vortices tend to merge to form a stronger vortex. The detection of merging vortices in downstream direction is similar to the described sequence for a single vortex, but detecting merging vortices in upstream direction results in detecting a splitting core line. The detection of a splitting vortex occurs in the corrector step. The enhanced analysis plane is separated in two regions. The inner region with the dimension of a single vortex core radius is used for the standard corrector step. The outer region up to the double vortex core radius is used for the detection of a splitting vortex. A new seed point is detected if vorticity and pressure values in points in the outer region are similar to the corrected point in the inner region. Figure 3 shows the corrector step with new seed point detection.

The corrector scheme based on the pressure minimum is only valid for non-cavitating flows. The pressure distribution in a cavitating area simulated with a Standard-Euler-Euler-approach and VoF approach is limited by the vapor pressure of the existing fluid. The pressure distribution on the analysis plane shows therefore almost the same pressure level.

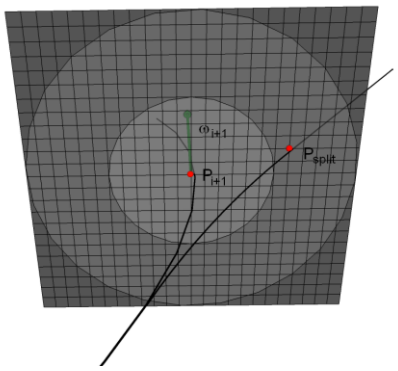


**Figure 3: Tracing of a splitting vortex core line**

$P_{split}$ represents a new seed point from which a new vortex core line is detected.

An alternative approach for pressure dependent vortex core detection is applied. This approach is called Vortfind and it is developed by Pemberton et al (Pemberton 2002). In this approach, the maximum vorticity is used to detect the core center and to correct the predicted point $P^*_{i+1}$. The procedure up to the corrector step is unchanged.

The Vortfind-technique is based on velocities and is based on a statement of Lugt (Lugt 1979): "A vortex is a rotating motion of a multitude of material particles around a common centre".

The points on the analysis plane (see Figure 2) are separated in three parts dependant on the velocity vectors.

$$0° \le \alpha < 120° \qquad \beta = 0$$
$$120° \le \alpha < 240° \qquad \beta = 1$$
$$240° \le \alpha < 360° \qquad \beta = 2$$

with $\alpha$ representing the angle between the velocity vector and a reference axis.

A length between points with differing $\beta$ is afterwards calculated to detect the vortex core.

$$l = p^2 + q^2 + r^2 \tag{3}$$

The vortex core point is placed at the location where *l* has a minimum. This detection method is recommended for cavitating flows but the computational effort is much higher than in the corrector step based on a minimum pressure or a maximum vorticity.

### 2.3 Combination

The combination of vortex detection and vorticity confinement results in a new established variable $\gamma$. The range of $\gamma$ is similar to the volume fraction $0 \le \gamma \le 1$ and depends on the distance between cell centers and detected vortex core lines.

$$\gamma = 1 - \left(\frac{l}{3r_v}\right)^n \text{ if } l \le 3r_v \tag{4}$$

$$\gamma = 0 \text{ if } l > 3r_v \tag{5}$$

$l$ is here the distance between the local cell centre and the nearest vortex core line, $r$ is the vortex core radius in the nearest vortex core line. $\gamma$ is only in regions where the distance $l$ is less than the triple core radius unequal to zero. This marks regions for the use of vorticity confinement. The transition area is smoothed to reduce numerical instabilities and to avoid unphysical pressure and velocity gradients.

## 3 CAVITATION MODELLING

The fluid is considered as a binary mixture as in the Volume-of-Fluid based models. The liquid base (index *l*) consists of the water and the homogenously distributed air. The other phase is the vapor (index *v*). Then the mixture density can be written as the sum of the partial densities

$$\rho = \rho_l + \rho_v \tag{6}$$

The liquid phase is modeled by a continuous Euler approach. Therefore an additional field variable, the volume fraction of the vapor, is needed. It is defined by

$$\alpha = \frac{V_v}{V_v + V_l} \tag{7}$$

where $V_v$ is the volume of vapor per unit volume and $V_l$ is the volume of liquid per unit volume. The cell volume is set as unit volume. Then the volume fraction is in the range of $0 \le \alpha \le 1$ and the mixture density can be calculated by $\alpha$ in the following way

$$\rho = \alpha\rho_v + (1-\alpha)\rho_l \tag{8}$$

The vapor phase is described with a Lagrangian approach. It is modeled by individual spherical bubbles of variable radius R, which represent ensembles consisting of a huge amount of physical bubbles. The set of equations defining the motion of the bubbles are

$$m_a \frac{dv_b}{dt} = F_{drag} + F_{press} + F_{vol} + F_{shear} + F_{bouy} \tag{9}$$

$$\frac{dx_b}{dt} = v_b \tag{10}$$

with the added mass $m_a = \frac{1}{2}\rho_l V_b$. The following forces are considered; see Abdel-Maksoud (2010) for details. The drag force:

$$F_{drag} = c_D \frac{\rho_l}{s} |v - v_b| (v - v_b) A_b \tag{11}$$

with the drag coefficient $c_D$, the fluid velocity $v$, bubble velocity $v_b$ and the projection area of the bubble $A_b = \pi R^2$. Important in vortical flows is the pressure gradient force:

$$F_{press} = -\frac{3}{2} V_b \nabla p. \tag{12}$$

The force due to volume variation of a bubble can be written as:

$$F_{vol} = \rho_l 2\pi R^2 \frac{dR}{dt}(v - v_b) \tag{13}$$

and the shear or Saffman force is represented by:

$$F_{shear} = c_L \frac{\rho_l}{2}(v - v_b)|v - v_b| A_b \tag{14}$$

with the lift coefficient $c_L$. The buoyancy force is given by:

$$F_{buoy} = (\rho_b - \rho_l) g V_b \tag{15}$$

The time integration of the Lagrangian equations is based on a Crank-Nicholson scheme. If a bubble reaches a rigid boundary, its velocity is set to the flow velocity at that position.

The dynamics of the bubble radius is described by the Rayleigh-Plesset equation:

$$\ddot{R} + \frac{3}{2}\dot{R}^2 = \frac{1}{\rho} \cdot \tag{16}$$

$$\left[ p_v + p_{g0}\left(\frac{R_0}{R}\right)^{3k} - p_\infty - \frac{2\sigma}{R} - \frac{4\mu\dot{R}}{R} + \frac{\rho}{4}(v - v_b)^2 \right]$$

Here $\sigma$ is the surface tension, $p_{g0}$ is the initial pressure of the non-condensable gas inside the bubble, $k$ is the isentropic coefficient, and $p_\infty$ is the local fluid pressure. This pressure is calculated by a surface-averaged pressure (SAP) formulation.

The fluid and the vapor phase are coupled by the vapor volume fraction $\alpha$. Their value is determined in the following way: the volumes of the bubbles located in a cell is summarized and divided by the cell volume; if the summarized volume is larger than the cell volume, this part is transported to the neighboring cell in direction of the mean bubble velocity.

The developed algorithm for consideration of the interaction between both phases consists of the following steps:

- Solve the Navier-Stokes equation
- Solve the Lagrange and Rayleigh-Plesset equation for each single Lagrangian bubble
- Calculate the continuous vapor volume fraction from the vapor volume of the discrete bubbles and calculation of the mixture density from Eq. (7)
- Repeat these steps until the solution is converged, and then go to the next time step

## 4 NUMERICAL METHODS

The Finite-Volume Navier-Stokes procedure *FreSCo*$^+$ uses a segregated algorithm which is based on the strong conservation form of the momentum equation and employs a cell-centered, co-located storage arrangement for all transport properties (Rung 2009). The procedure can be used in conjunction with structured-grid and unstructured-grid discretizations, based on arbitrary polyhedral cells, including cells with hanging nodes.

The implicit numerical approximation is second-order accurate in space and time. Integrals are approximated using the conventional mid-point rule. Diffusion terms are subsequently approximated using second-order central differences, whereas advective fluxes are approximated using high-order bounded (monotonic) schemes. The latter are applied in scalar form by means of a deferred correction approach.

Various turbulence-closure models are available with respect to statistical (RANS) approaches. Two-phase flows are addressed by interface-capturing methods based upon the Level-Set or Volume-of-Fluid (VOF) technique. Fully conservative interface-sharpening techniques are optionally available.

Linear equations systems are solved by means of Krylov-subspace methods offered by the PETSC library. Since the data structure is generally unstructured, suitable preconditioned iterative sparsematrix solvers for symmetric and non-symmetric systems (e.g., GMRES, BiCG, QMR, CGS, BiCGStab) can be employed. The algorithm is parallelized using a domain-decomposition technique based on a Single Program Multiple Data (SPMD) message-passing model (i.e., each process runs the same program on its own subset of data). Inter-processor communication employs the MPI communications protocol. Load balancing is achieved using the ParMETIS partitioning software.

## 5 RESULTS

### 5.1 Vortex detection

Vortex detection was first tested on artificial vortices produced by a velocity boundary condition at the inlet. The velocity profile of a Burgers vortex given as follows:

$$v_\varphi = \frac{\Gamma}{2\pi r}\left(1 - e^{-1.256\frac{r}{a^2}}\right) \tag{17}$$

where $r$ is the radius, $a$ is the core radius of the vortex and $\Gamma$ is the circulation. This velocity profile is added to a cylindrical computational domain with 200000 hexahedral cells.

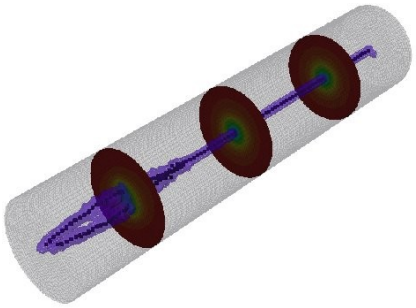

**Figure 4: Detection of two Burgers vortices**

Figure 4 shows the detection of two Burgers vortices. The seed point detection takes place in the middle of the

computational domain and the tracing occurs upstream as well as downstream. The detection of the joining two vortices is successful. The detection in this area is done in upstream direction, which results in a detection of a split of the vortex core line. The isosurface additionally shows the area in which the vorticity confinement formulation is considered.

### 5.1 Cavitation model

The cavitation model was tested on a quasi 3-dimensional flow through a duct. The calculated flow velocity and volume fraction using the two-way coupling between the Lagrangian bubbles and the flow field can be seen in Figure 5.

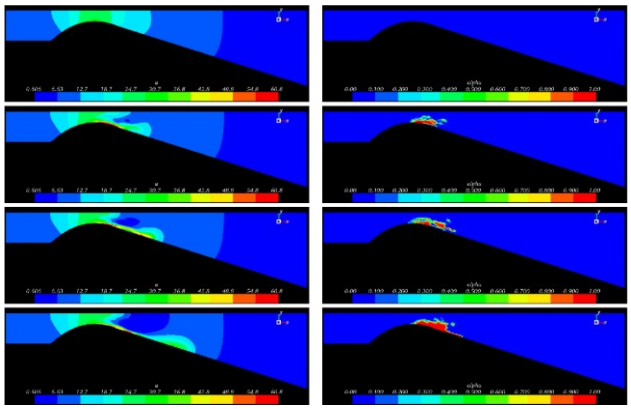

**Figure 5: Euler-Lagrange-Simulation, flow velocity in axial direction (left), volume fraction (right)**

The consideration of interaction between the Lagrangian bubbles and the flow field leads to a fully unsteady result, while a one-way coupling calculation with a passive bubble transport produced a stationary result. The Lagrangian bubbles start to grow in the high velocity region where the pressure falls below the vapor pressure. A vapor phase is formed in this region, which can be qualitatively seen in the left part of Figure 5. But validation of this cavitation model is yet to be done.

### 5.2 Propeller E779a

The vorticity confinement method in combination with vortex detection is coupled to the Euler-Lagrange cavitation model and tested on a four-bladed propeller (INSEAN E779a). The main dimensions of the model-scale propeller are:

Diameter: $d_m = 227.27mm$

Expanded Area Ratio: $A_E / A_0 = 0.689$

No. of blades: Z=4

Pitch / diameter ratio: $P_m / d = 1.1$

Rake: 4°3”

Water temperature: 25°C

Cavitation number: $\sigma = \dfrac{p_{ref} - p_v}{\frac{1}{2}\rho u_\infty^2} = 1.2$

Calculations were carried out for J=0.65. This leads to an inflow velocity of $u_\infty = 5.32\,m/s$ and a rotational speed of $n = 36s^{-1}$. The applied cylindrical numerical grid of hexahedral cells consists of 1.2 mil. nodes.

Calculations were first carried out with the Euler-Lagrange cavitation model without considering the vorticity confinement method. The start areas for the bubbles are placed in front of the blade tips to examine the tip vortex cavitation.

Figure 6 shows the pressure distribution on the propeller surface. The blue-colored isosurface shows the vapor pressure. Cavitation bubbles can be seen inside the isosurface where the local pressure is below the vapor pressure. No cavitation bubbles can be found in the tip vortices although there is a refined mesh in this area. The mesh resolution in this region is insufficient to reproduce the low pressure region of the tip vortices.

The introduced vorticity confinement method in combination with vortex detection is applied to improve the reproduction of the tip vortices in the numerical calculation. First, vortex core centers are determined to identify the necessary areas of interest. Figure 7 shows the detected vortex core centers of the tip vortices. The higher distance between the detected core centers in the downstream area of the tip vortices is a result of the change of the mesh resolution.

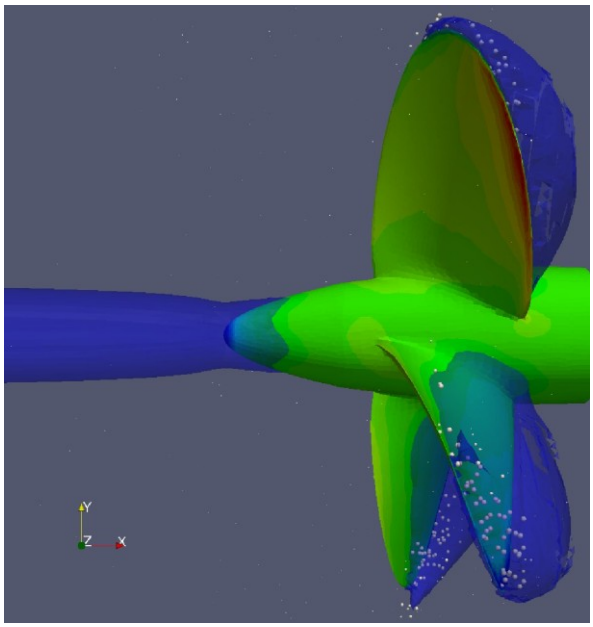

**Figure 6: Pressure distribution on the propeller surface and Lagrangian cavitation bubbles (no vorticity confinement)**

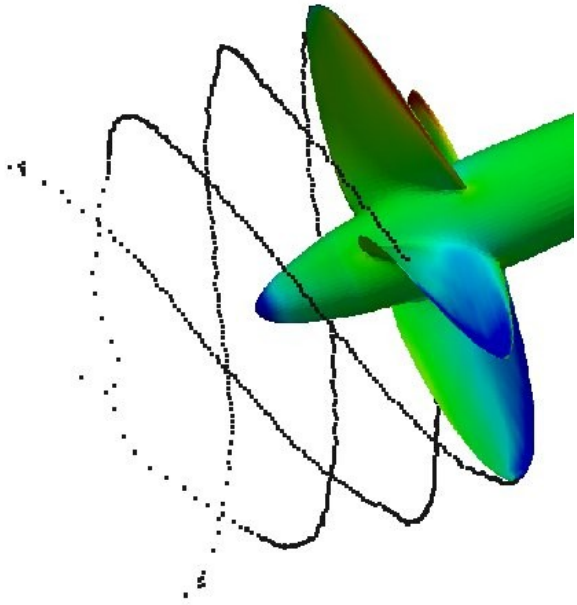

**Figure 7: Detected vortex core centers of tip vortices**

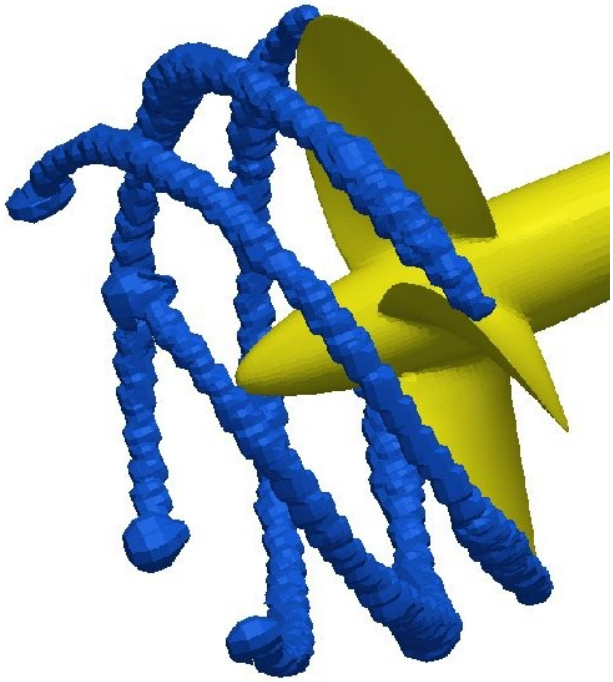

**Figure 8: Isosurface $\gamma = 0.01$ of detected vortex area**

Figure 8 shows the isosurface of $\gamma = 0.01$. The flow inside this isosurface is manipulated by the vorticity confinement method. It can be seen that only the areas of interest are manipulated. Manipulation (e.g., in the boundary layer) is completely disabled. Influence on the propeller thrust and propeller torque due to VC is insignificant. Calculated thrust and torque coefficients can be seen in Table 1.

**Table 1: Thrust and torque coefficients for J=0.65**

| | $K_T$ | $10*K_Q$ |
|---|---|---|
| Measurements | 0.29 | 0.51 |
| Calculation | 0.26 | 0.47 |
| Calculation with VC | 0.26 | 0.47 |
| Calculation with VC and Euler-Euler cavitation model | 0.17 | 0.33 |
| Calculation with VC and Euler-Lagrange cavitation model | 0.25 | 0.43 |

Figure 9 shows results of the calculation with the Euler-Lagrange cavitation model and the vorticity confinement method with vortex detection. Lagrangian bubbles can now be seen in the tip vortices. The hub vortex is additionally detected.

The interaction between the Lagrangian bubbles and the fluid flow is included in the simulation by a variable mixture density as described in Section 3. Figure 10 illustrates the vapor volume fraction, which is calculated from the volumes of the Lagrangian bubbles.

The number of Lagrangian bubbles can explain the discrepancies of $K_T$ and $K_Q$ between the Euler-Euler simulation and the Euler-Lagrange simulation. The number of Lagrangian bubbles in this computational approach is kept low to reduce the computational effort. Each Lagrangian bubble therefore represents a huge amount of physical bubbles. Using a larger amount of Lagrangian bubbles and the associated reduction of represented physical bubbles per Lagrangian bubble will show a more accurate determination of the vapor volume fraction and a more accurate $K_T$ and $K_Q$, see Table 1.

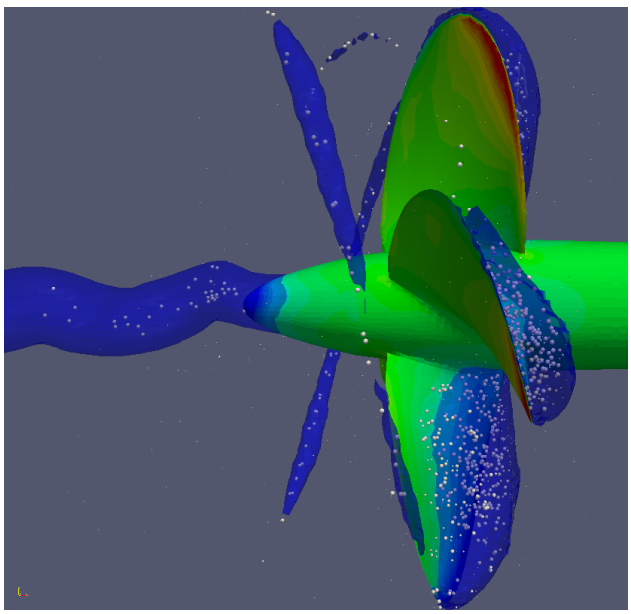

**Figure 9: Pressure distribution on the propeller surface and Lagrangian cavitation bubbles with vorticity confinement**

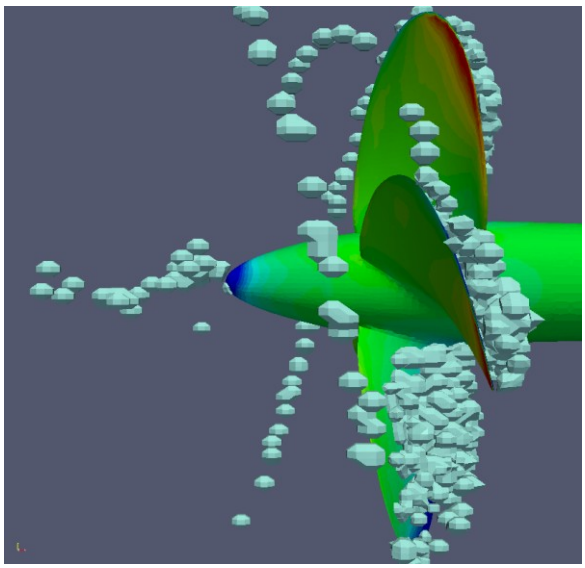

**Figure 10: Pressure distribution on the propeller surface and vapor volume fraction calculated by the Lagrangian bubbles**

The advantages of the vorticity confinement formulation in combination with a vortex detection algorithm can also be used in common Euler-Euler-based cavitation models. Results of these calculations can be seen in Figure 11 and Figure 12.

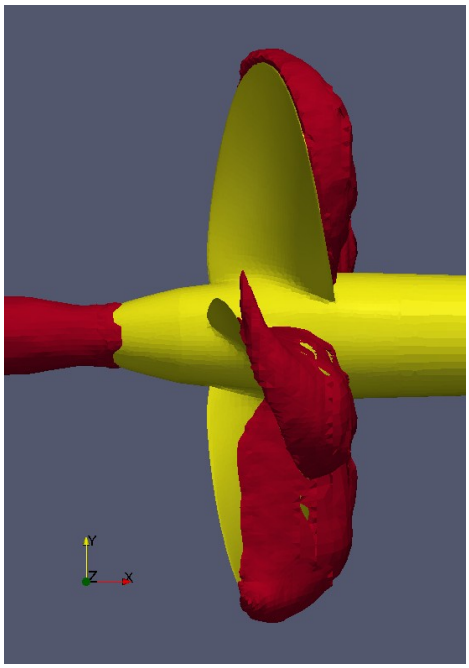

**Figure 11: Vapor volume fraction calculated by Euler-Euler cavitation model without applying the vorticity confinement**

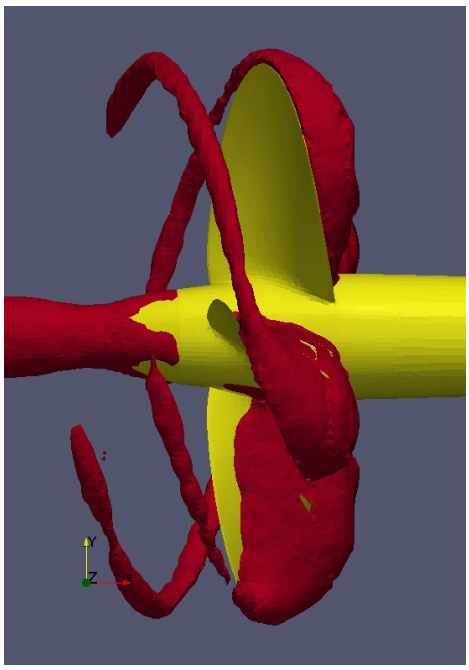

**Figure 12: Vapor volume fraction calculated by Euler-Euler cavitation model including vorticity confinement**

A significant increase in vapor volume can be seen in the vortex core regions of the tip vortices by the applying of the introduced combination of vorticity confinement and vortex detection.

### 6 Conclusions

The two-phase flow caused by cavitation has a strong influence on the performance of marine propulsors. Main objective of this numerical study is the investigation of numerical aspects influencing the vortex dominated flows of cavitating propellers. Computations of the flow behavior on real propeller configurations require high grid resolution to capture important details of the cavitating flow. Insufficient resolution increases the numerical dissipation of vortices generated in the tip region. An efficient method to overcome the problem of the unphysical decay of the strength of the vortices is the combination of the vorticity confinement formulation and vortex detection methods.

The Euler-Euler methods for predicting cavitation perform sufficiently well in regions of moderate flow changes and weak cavitation but fail in zones of strong, vortical flow, as, e.g., in ranges of tip vortices of propellers. Reasons for this are the limited grid resolution and the restrictions of these methods such as the transport of the vapor bubbles with the fluid velocity along streamlines and the inadequate consideration of bubble dynamics.

The alternative Euler-Lagrangian concept is more expensive compared to the Euler-Euler approach, but enables detailed formulations for movement and dynamics of single bubbles.

In the most cases, one-way coupling is usually applied in Euler-Lagrangian methods (i.e., the vapor does not influence the liquid phase). One reason for often

application of one-way coupling compared to two-way coupling is the relatively complex formulation of two-way coupling. This is necessary in order to have an accurate and numerical stable modeling of the interaction between discrete bubble phase and continuous fluid phase.

However, two-way coupling is required when the regions of the vapor phase become large and thus the influence on the carrier flow remarkable. Therefore, a two-way coupling concept between the phases is presented in this study. It is based on the definition of volume fractions, derived from the bubble distribution inside and around a computational cell.

The capability of developed concepts for two-way coupling, vortex confinement and vortex detection is demonstrated for a propeller geometry.

The application of vortex confinement and vortex detection significantly improve the quality of the results of the two-way coupling in the vortex flow regions. The achieved results show that the developed methods allow the consideration of many important physical aspects of cavitating flows on ship propulsion systems.

## ACKNOWLEDGMENTS

This work has been supported by the German Research Society (DFG). The authors thank the *FreSCo*$^{+}$ team for the kind support.

## REFERENCES

Abdel-Maksoud, M., Hänel, D. & Lantermann, U. (2010). 'Modeling and computation of cavitation in vortical flow'. International Journal of Heat and Fluid Flow **31**, pp. 1065-1074.

Banks, D. C. & Singer, B. A. (1995). 'A Predictor-Corrector Technique for Visualizing Unsteady Flows'. IEEE Transactions on Visualization and Computer Graphics **1**, pp. 151-163.

Lugt, H. J. (1979). Wirbelströmung in Natur und Technik. Verlag Braun.

Pemberton, R. J., Turnock S. R., Dodd, T. J. & Rogers, E. (2002). 'A novel method for identifying vertical structures'. Journal of Fluids and Structures **16**(8), pp. 1051-1057.

Robinson, M. A. (2004). 'Application of vorticity confinement to inviscid missile force and moment prediction'. Proceedings of the 42nd AIAA Aerospace Sciences Meeting and Exhibit.

Rung, T., Wöckner, K., Manzke, M., Stück, A., Brunswig, J. & Ulrich, C. (2009). 'Challenges and Perspectives for Maritime CFD Applications'. Jahrbuch der Schiffbautechnischen Gesellschaft **103**.

Steinhoff, J. & Upperhill, D. (1994). 'Vorticity Confinement: A New Technique for Computing Vortex dominated flows'. Frontiers of Computation Fluid Dynamics.